Predicting wheat production at regional scale by integration of remote sensing data with a simulation model

Raymond E.E. Jongschaap, Léon S.M. Schouten

Agron. Sustain. Dev. 25 (2005) 481–489

DOI: 10.1051/agro:2005048

Original article

Predicting wheat production at regional scale by integration of remote sensing data with a simulation model

Raymond E.E. JONGSCHAAP[a]*, Léon S.M. SCHOUTEN[b]

[a] Wageningen University and Research Centre, Plant Sciences Group, Plant Research International BV, PO Box 16, 6700AA Wageningen, The Netherlands
[b] Synoptics Ltd., PO Box 117, NL-6700AC Wageningen, The Netherlands

(Accepted 6 June 2005)

Abstract – Optical remote sensing satellite data (SPOT HRV XS, Landsat 5 TM) were used to estimate winter wheat area in a pilot area of 5 × 5 km in the Southeast of France. The approach was scaled up to a larger area of 45 × 50 km and finally to the regional level covering several departments. Microwave remote sensing data (ERS SAR C-band) were used to estimate regional wheat flowering dates to calibrate a wheat growth simulation model used to calculate wheat yields, subsequently used to estimate regional wheat production. Soil maps were used to spatially vary model input parameters for the region. Wheat area could be estimated with more than 80% users' accuracy and model-based estimates of regional wheat production were in agreement with agricultural statistics. These results demonstrate that results from point-based simulation models can be applied at spatially higher levels with the aid of remote sensing data.

Landsat / SPOT / ERS SAR C-band / classification / simulation model / calibration / point to region scaling / wheat / flowering date

1. INTRODUCTION

Timely and accurate information on crop and soil status is critical for management decision-making in arable farming to optimise crop production and to reduce environmental pollution. Normally, field observations are performed repeatedly, at specific crop stages, to enable timely intervention with appropriate management measures. Availability of up-to-date and accurate information on the crop-soil status at the (sub-) plot or farm scale will benefit farmers, whereas local and regional policy makers or food processing industries will be more interested in regional crop production estimates. Sofar, both, remote sensing applications and dynamic simulation models have played significant, but different (and mostly separate) roles in generation of such information (Jones et al., 2001). Combining remote sensing applications and dynamic simulation models has been explored in several studies (Bouman, 1991; Van Leeuwen, 1996; Clevers et al., 2002; Prévot et al., 2003), but these approaches aimed at quantitative biomass, leaf area index and canopy nitrogen estimates from remote sensing data to reconstruct crop growth curves used for calibrating dynamic simulation models at field scale. Another more direct technique to integrate remote sensing observations in crop growth simulation models has been demonstrated by others (Boegh et al., 2004; Jongschaap, 2005). Jongschaap (2005) used remote sensing observations of model variables (leaf area index and canopy nitrogen) for "run-time calibration"; i.e. resetting the simulated value with the value estimated from remote sensing data. This approach resulted in more accurate predictions of the dynamics of characteristics of the crop-soil system, including variables that were not directly adjusted. A more innovative and useful combination of both remote sensing and simulation modelling integrates knowledge of lower-scale processes in the crop and soil systems, captured in simulation models, with the possibility to analyse effects at higher (spatial) scales. Therefore the aim of this study was to find a method that allows integrating simulation results at point or field scales and use remotely sensed data to estimate grain production at higher (regional) scales. To reach this objective, optical remote sensing data is used for the classification of winter wheat fields and radar remote sensing data are used to establish a regional estimate for flowering date of winter wheat.

Remote sensing applications originally dealt with classification themes, such as identification and mapping of (originally military) objects. Classification is still of major importance in civil remote sensing applications (Lloyd et al., 2004; De Wit and Clevers, 2004), but quantification of object variables from remotely sensed information has become increasingly important (Moreau and Le Toan, 2003). To transform remote sensing signals into useful information, spectral "vegetation indices" (VI) are computed, e.g. by combining visible and near infrared bands. VI are significantly related to important crop characteristics, such as leaf area index (LAI), biomass and chlorophyll content (Guyot et al., 1988; Jago et al., 1999; Thenkabail et al.,

* Corresponding author: raymond.jongschaap@wur.nl

2000; Jongschaap and Booij, 2004). One of the VI that is well related with (green) biomass is the Normalized Difference Vegetation Index (NDVI; Rousse et al., 1974) that can be used to distinguish bare soil from vegetation, and to filter grasslands from winter crops if the timing of the image is well chosen. As a consequence of using (broad band) satellite sensors, operating at lower spatial resolutions than spectral field-based sensors, relations between VI and crop-soil characteristics are less accurate. Another disadvantage of airborne and satellite remote sensing is the spatially distributed atmospheric distortion, which is practically absent in field-based or airborne remote sensing observations. Furthermore, sensors that operate in the visible domain may be hampered by cloud cover, which may be a problem for the calculation of VI at important crop development stages. It is assumed that spectral and spatial resolution of SPOT HRV XS (multispectral) and Landsat 5 TM provide enough detail, and that cloudless images can be selected from appropriate time windows. At the appropiate wavelengths, radar data are not hampered by cloud cover. Target objects in size exceeding the radar wavelengths result in radar backscattering, whereas smaller objects attenuate the radar signal (Hamacher, 2000; Macelloni et al., 2002). The ERS SAR C-band radar data that are used have wavelengths of about 5.6 cm, so the radar signal is expected to attenuate more strongly with increasing (wet) biomass, but will show an increase with wheat ear layer development and drying of the crop canopy towards maturity.

In this study, spaceborne remote sensing observations (SPOT HRV XS, Landsat 5 TM and ERS SAR radar data C-band) are used and combined with crop growth simulation modelling to estimate regional production volumes, in this case for winter wheat (*Triticum aestivum* L.) that is grown in the Southeast of France. The advantage in this methodology is that regional grain production estimates can be provided at an early stage, even before harvest.

2. MATERIALS AND METHODS

The approach for integration of remote sensing imagery and crop growth simulation to arrive at regional estimates of wheat production comprise the following steps:

1. Optical remote sensing data (SPOT HRV XS and Landsat 5 TM) are used to locate winter wheat crops in the region.

2. Radar remote sensing data (ERS-SAR C-band) are used to determine wheat flowering dates for the region.

3. Field observations from pilot areas are used to calibrate a wheat growth model to local conditions.

4. Flowering dates as found in step 2 and 3, in combination with regional soil data, are used to extrapolate the simulation model from a point-based to a regional application.

5. Potential and sub-optimal conditions for wheat growth are assumed to determine the yield gap, defined as the difference between (simulated) potential production and (simulated and observed) actual production (Van Ittersum and Rabbinge, 1997).

6. Actual production statistics from the production region are used to evaluate simulation results.

Table I. Specification of the optical remote sensing data.

Satellite / Sensor	Scene coordinates	Date
SPOT1 HRV XS	K 49 – J 261	February 1st, 1997
Landsat 5 TM	path 196 row 30	April 13th, 1997
SPOT2 HRV XS	K 49 – J 261	July 7th, 1997

2.1. Test sites

The calibration and validation test sites were situated in the Southeast of France near Avignon, in the department *Bouches-du-Rhône*. Model calibration (step 3) was performed on data from a pilot site of 5 × 5 km: *Alpilles* – named after the small mountain chain that borders the area in the south. A larger area in the same region (45 × 50 km) was used to extrapolate model simulations (step 4). This area is further referred to as *Arles* – named after the town that is situated in this region. The approach was further validated (step 6) at the department level (regional scale) in the regions *Midi-Pyrénées* (*MP*) and *Provence-Alpes-Côte d'Azur* (*PAC*).

The experimental fields in *Alpilles* were situated in a very flat area with an altitude around 10 meters above sea level. Main crops are wheat, maize, sunflower and grassland. Some minor crops are tomatoes, artichoke and alfalfa. Fields at the test sites have an average size of ca. 200 × 200 m, which is large enough to extract pure pixels from high spatial resolution satellites such as SPOT HRV XS, Landsat 5 TM and ERS-SAR. *Alpilles* is representative for the *Arles* region and for *MP* and *PAC* with regard to cropping patterns and crop management.

2.2. Classification of wheat fields using optical imagery

The growth patterns of winter crops form the basis for winter wheat classification in the *Alpilles* pilot area and in the larger *Arles* region by using the sequential information of three optical satellite images acquired during the growing season. The optical images that were required are a Landsat 5 TM image and two SPOT HRV XS images (Tab. I).

Atmospheric correction using the 6S software (Vermote et al., 1997) was applied before the geometrical correction. The aerosol model was based on actual atmospheric optical thickness measurements during satellite overpass, using a sun photometer installed at the *Alpilles* test site.

In wintertime, arable fields are normally not covered by significant amounts of crop biomass, unless pastures or winter crops are grown. At the end of the summer growing season (October/November in Europe) winter crops may be sown, that can accumulate a substantial amount of green biomass before crop growth and development cease due to decreasing temperatures and reduced solar radiation. In early spring (March/April in Europe), when temperatures are rising and incoming solar radiation increases, these winter crops benefit from their advanced development: the green canopy is able to capture early incoming radiation and a partially developed root system can take up water and nutrients from the soil.

The Normalised Difference Vegetation Index or NDVI (Rouse et al., 1974) identifies green biomass and is calculated from the visible and near infrared bands provided in SPOT

HRV XS and Landsat 5 TM images. Green plots, with high NDVI values, comprising green winter wheat fields and green pastures, were identified from the Landsat 5 TM image and the February SPOT1 image by unsupervised classification (isodata clustering with 50 classes that were identified and clustered by field observations in the *Alpilles* pilot area). These fields were sampled again in the July 1997 SPOT2 image, taken after winter wheat harvest, so that winter wheat fields show up as bare soil in the remote sensing image. By looking at the difference between summer images and winter images, winter wheat fields were identified as the only winter crop grown in this region. The classification result was majority-filtered (box size 3 × 3) to assign values of neighbouring pixels to isolated pixels if these were situated within an identified wheat field. Field observations and ancillary data were used to calculate the users' accuracy of the above method in the *Arles* region, i.e. dividing the number of correctly classified samples by the total number of samples that were classified as belonging to that category (Story and Congalton, 1986).

2.3. Radar detection of flowering in wheat

Flowering is a very important and a distinctive phenological event in wheat production that marks the start of grain growth in ears at the top of the canopy. Ear biomass per unit area increases over time through the increase in the number of flowering plants, through grain growth from current photosynthesis products, and through translocation of carbohydrates from temporary storage organs (mainly stems) to the developing grains. Growing ears significantly affect radar back scatter signals, as their presence and increasing biomass at the top of the canopy modify crop geometry and crop moisture distribution and hence, attenuation of the radar signal (Hamacher, 2000; Macelloni et al., 2002).

With the Cloud-model (Eq. (1)), radar back scatter and attenuation of a vegetation-soil system can be simulated (Attema and Ulaby, 1978). In the model, vegetation and soil are represented as clouds of water drops, and radar back scatter (γ) depends on the radar beam incidence angle (θ) and on the moisture content and its distribution in vegetation (C-term) and soil (G-term). High values for W (canopy water content per unit soil surface) mask the influence of the soil term.

$$\gamma = C_\theta \cdot \left(1 - e^{\left(\frac{-D \cdot W}{\cos(\theta)} \right)} \right) + G_\theta \cdot e^{\left(m \cdot k \frac{-D \cdot W}{\cos(\theta)} \right)} \quad (1)$$

with γ = radar back scatter per unit projected area ($m^2\ m^{-2}$), C = back scatter of an optically dense vegetation cover ($m^2\ m^{-2}$), = incidence angle (°), D = crop moisture extinction coefficient (m^{-1}), W = canopy water content per unit soil surface (kg m^{-2}), G = back scatter of dry soil ($m^2\ m^{-2}$), m = volumetric soil moisture content (cm^3 water cm^{-3} soil), K = top soil moisture extinction coefficient (m^{-1}).

ERS time-series (Tab. II) were selected as wheat signatures are reported to behave consistently in C-band VV (even under varying soil moisture conditions), contrary to those of crops with more planophile oriented leaves such as sugar beet, potato and maize (Van Leeuwen, 1996).

Table II. Specification of the radar (ERS1 SAR) remote sensing data.

Date	Mode[a]	Orbit	Frame
December 19th, 1996	D	8707	2727
January 23rd, 1997	D	9208	2727
January 26th, 1997	A	9259	873
February 27th, 1997	D	9710	2727
April 6th, 1997	A	10261	873
May 8th, 1997	D	10712	2727
June 12th, 1997	D	11213	2727
July 17th, 1997	D	11714	2727
August 21st, 1997	D	12215	2727
September 25th, 1997	D	12716	2727

A = Ascending, D = Descending.

ERS radar beams in the C-band (at a frequency ≈5.3 GHz and with a wavelength ≈5.6 cm) acquire radar back scatter from objects larger than ≈5.6 cm. Broad leaves (such as sunflower leaves, sugar beet leaves and maize leaves) will produce C-band back scatter, in contrast to small-sized leaves (such as those of wheat and grasses). Instead, radar signals will attenuate in the vegetation biomass (Macelloni et al., 2002). The use of ERS time-series of winter wheat fields to identify crop phenological stages is legitimate, if values for crop moisture extinction coefficients (D) are relatively stable in time. Dry soil back scatter (G) is different for different soil types and may vary among studies. The relative contributions of crop water content (D) and soil moisture content (G) to radar back scatter signals (D:G) may vary between 83–96% (Tab. III). D and G parameter values were established for the *Alpilles* pilot area by fitting the Cloud-model to field observations.

As D-values appeared to be stable (Tab. III), a method was developed to detect flowering dates in wheat crops, based on the associated change in crop moisture distribution and crop geometry, with the flowering stage marking the point where aboveground water contents start to decrease and minimum radar back scatter can be expected (Hamacher, 2000). In the pre-flowering growth phase, canopy water content per unit soil surface area (W) increases with increasing biomass and the radar signal will be decreased due to attenuation by the canopy. After the onset of flowering, an optically dense vegetation cover of ear biomass starts to develop that prevents radar beams from penetrating deeply into the wheat canopy, thereby reducing the radar signal maximally. Fully developed ears may produce backscatter, and as soon as grains start to ripen, the moisture content of the crop decreases resulting in increased radar back scatter as the influence of the soil is no longer masked. The absolute minimum in the radar signal (i.e. at maximum attenuation) therefore denotes the maximum water content per unit surface area and hence flowering.

Regional dynamics of these phenological events can be detected by ERS (radar) remote sensing. Success rate increases if more comparable (wheat) fields are included in the detection procedure. Based on this approach, regional flowering dates have been estimated for simulation model calibrations with time-series of ERS (radar) data (taken in the period November 1996–May 1997). For the *Alpilles* area, 10 ERS radar images

Table III. Cloud model parameters K, D and G (See Eq. (1)) from various experiments.

K	D	G	Study area	Reference
0.035	0.4800	0.0863	Alpilles (France)	Prévot et al. (1998)
0.058	0.4501	0.0384	Alpilles (France)	Synoptics (1996)
0.078	0.4330	0.0186	Flevoland (Netherlands)	Bouman et al. (1999)
0.130	0.4338	0.0028	Alpilles (France)	Synoptics (1996)

Table IV. FAO/UNESCO legend unit 3139, its constituent soil codes and the interpretation for simulation purposes in Rotask v1.5.

Soil (code)	Texture (class)	Slope (class)	Area[a] (%)	Soil depth (cm)	Available water content (mm m^{-1})
Calcaric Fluvisols (Jc)	1	1	25	130	200
Gleysols (G)	2	1	20	130	200
Eutric Fluvisols (Je)	2	1	20	130	200
Cambisols (B)	2	2	10	130	190
Calcaric Fluvisols (Jc)	3	1	25	130	200

[a] Percentage of the soil legend unit area that is covered by the soil code.

were available of which 7 coincided with the wheat growth period. The 8 descending ERS-SAR images were co-registered (linear transformation to the file coordinates of one reference scene) and the 2 ascending images also. Subsequently all images were speckle-filtered (Gamma Maximum A Posteriori filter; Lopez et al., 1993) that best retains edge and line features, with a window of 7 × 7 pixels that is appropriate for the medium-sized wheat fields. Remote sensing time-series were transformed to the Lambert III projection, the standard map projection for this part of France. All ERS-images were re-sampled (nearest neighbour) to pixels representing 25 m^2. Classified SPOT images were overlaid with ERS images to generate mean back scatter (DN values) for winter wheat fields only.

2.4. Wheat growth simulation model

Winter wheat simulations were performed with the mechanistic crop growth model *Rotask* (Jongschaap, 1996), that uses (simple) algorithms based on knowledge of the underlying physical, physiological and biochemical processes. The model quantifies water fluxes (precipitation, irrigation, run-off, soil evaporation, transpiration and drainage), nitrogen fluxes (mineralization/immobilisation during soil organic matter decomposition, mineralization from dead plant material, (in-)organic fertilisation, wet deposition, leaching and root nitrogen uptake by mass flow and diffusion), for fallow or field crop rotation systems. Light interception and heat accumulation govern crop growth and development, respectively. Crop nitrogen contents may vary as a result of variations in nitrogen availability. Management decisions accounted for in the model refer to ploughing (date, depth), incorporation of organic fertiliser (date, rate, type), and application of inorganic fertiliser (date, rate, type), sowing (rate, depth), irrigation (date, rate) and harvest (date, method). Crops currently included in the model are wheat, sugar beet, potato, barley, rape-seed and maize. For this study, simulations were performed for winter wheat only. The model has been calibrated for winter wheat and for the soil conditions of the *Alpilles* pilot area, using 1996, 1997 and 1998 field data (Jongschaap, 2000; ReSeDA, 2000).

2.5. Up-scaling from point to regional level

Two methods were applied to scale-up point-based simulations to the regional scale. Firstly, sowing dates were varied over the month of November in 1996 to introduce variation in the model variable "sowing date", to mimic the observed variable sowing dates of winter wheat in the area. Temperature sums calibrated for the Alpilles pilot area were applied for the periods sowing to flowering and flowering to maturity.

Secondly, the spatial variability in soil characteristics was derived from the FAO/UNESCO 1:5,000,000 Soil Map of the World (FAO, 1995). Higher resolution soil maps of the region are available from different sources, but in our approach we wanted to use broad-scale soil information to be applied at regional level. The soil map resolution of 5 arc minutes results in a grid of 10 × 10 km at the latitude of the *MP* and *PAC* region. On the soil map, 3 legend units were identified in the region: 3086 (17%), 3139 (80%) and 6498 (3%). The remote sensing data showed that only unit 3139 contained wheat fields. Derivation of the relevant soil characteristics for the simulation model, available water content and slope (Tab. IV), resulted in 10% of its area having a water storage capacity of 190 mm m^{-1} and a slope exceeding 8%, while the remainder had a water storage capacity of 200 mm m^{-1} and a slope below 8%.

The simulation model was executed for 3 production situations with significantly different grain yields (Van Ittersum and Rabbinge, 1997), because of production constraints that were included in the model:

- Potential production; wheat growth and development are governed only by crop characteristics, intercepted radiation and average daily temperatures.

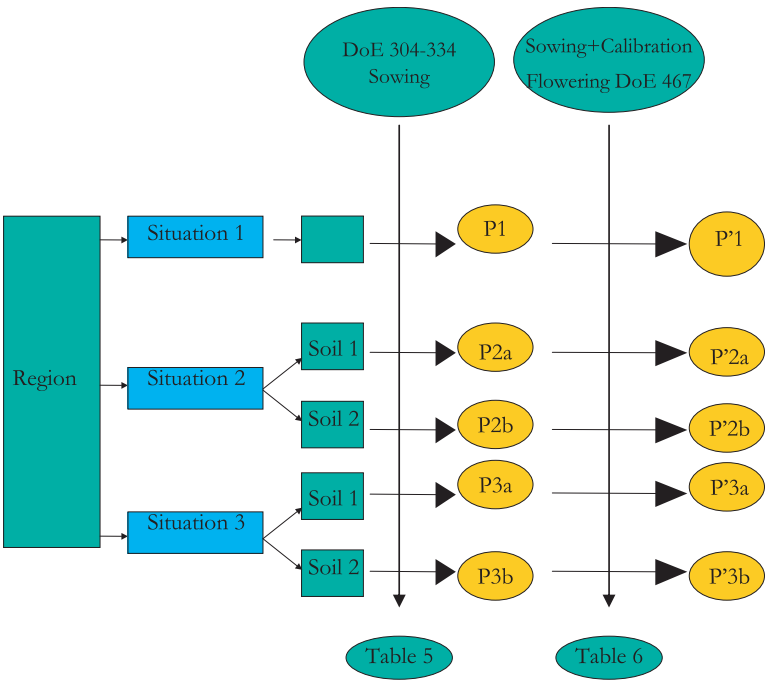

Figure 1. Simulation scheme for estimation of regional grain production P, after determination of wheat area and soil types and estimation of regional flowering date.

- Water-limited production; as 1, but accounting for inadequate soil moisture supply during crop growth: daily assimilation rates are reduced proportionally to daily relative crop transpiration deficits.
- Nitrogen- and water-limited production; as 2, but accounting for the effect of inadequate soil nitrogen supply during crop growth, which may cause canopy nitrogen contents to reach critical values, resulting in reduced assimilation rates.

When water and nitrogen supply from natural sources do not meet crop requirements, production situation 1 results in higher yields than production situation 2 (yield gap for production situation 2), which in turn gives higher yields than production situation 3 (yield gap for production situation 3). The production situations were implemented without irrigation water supply (situations 2 and 3) and without nitrogen fertiliser application (situation 3). Irrigation and fertiliser application data were available for the calibration data set, but not for extrapolation to the regional scale.

Hence, the simulation experiment was set up as follows (Fig. 1): the region was first filtered for winter wheat fields, and subsequently the simulations were performed for the 3 production situations. The two soil types were used in production situations 2 and 3 only, as for production situation 1 soil characteristics are not taken into account. Sowing dates were varied over the month of November 1996 (Date of Experiment (DoE): 304–334), leading to grain yields P (t ha^{-1}). After calibration of the temperature sums between sowing and flowering to DoE 467 (estimated from ERS data), grain yields were P' (t ha^{-1}). Multiplication by the estimated area resulted in regional estimates of winter wheat grain production (t).

Simulation results per soil type are given as Final Grain Yield (FGY, Dry Matter (air-dry) in t ha^{-1}), with a standard deviation resulting from the simulated variation in sowing date. Multiplication of FGY with the wheat area identified through optical remote sensing resulted in regional grain yield estimates for the 1997 season.

3. RESULTS AND DISCUSSION

3.1. Remote sensing estimates of wheat area and flowering date

About 145 ha of wheat fields in the *Alpilles* pilot area were used to validate the remotely sensed unsupervised classification process, which resulted in a users' accuracy > 80% (Story and Congalton, 1986). In the *Arles* region of 45 × 50 km, about 3000 ha of winter wheat fields were identified (Fig. 2), i.e. 1.4% of the 211 800 ha of wheat reported for the *MP* and *PAC* region.

The crop moisture extinction coefficient (D) of the Cloud-model (Attema and Ulaby, 1978) was stable over time and its value agreed with those from other studies (Tab. III), although reported standard errors are relatively large.

Nonetheless, ERS (radar) time-series are useful for estimation of wheat flowering dates in the region, as average back scatter behaviour of radar time-series of winter wheat fields is consistent (ESA, 1998; Hamacher, 2000).

A 5th order polynomial function fitted best through the 10 points representing back scatter values of winter wheat fields (Fig. 3). Theoretically, the 5th order agrees with the

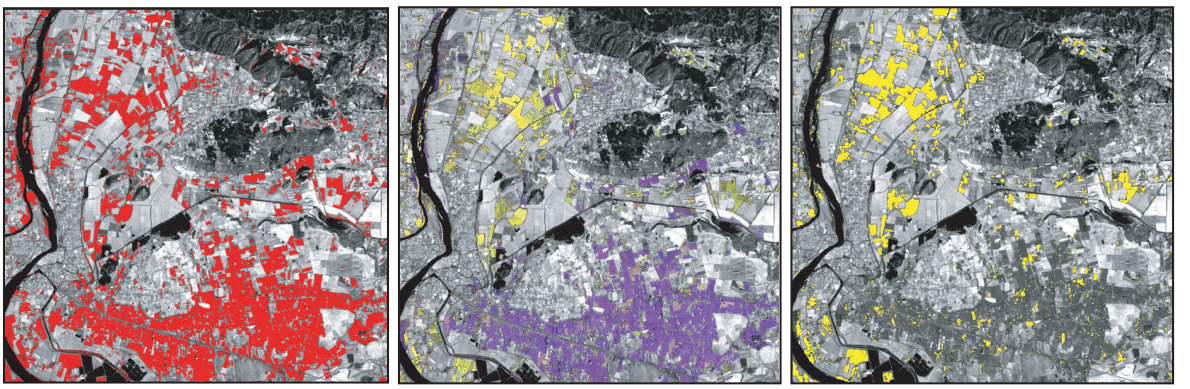

Figure 2. Classification results for the Alpilles test site (45 × 50 km): Green biomass detection by a combined February SPOT1 image and April Landsat 5 TM image (left), harvested wheat fields show up as bare fields on July SPOT2 image (middle) and resulting wheat fields after majority box (3 × 3) filtering (right).

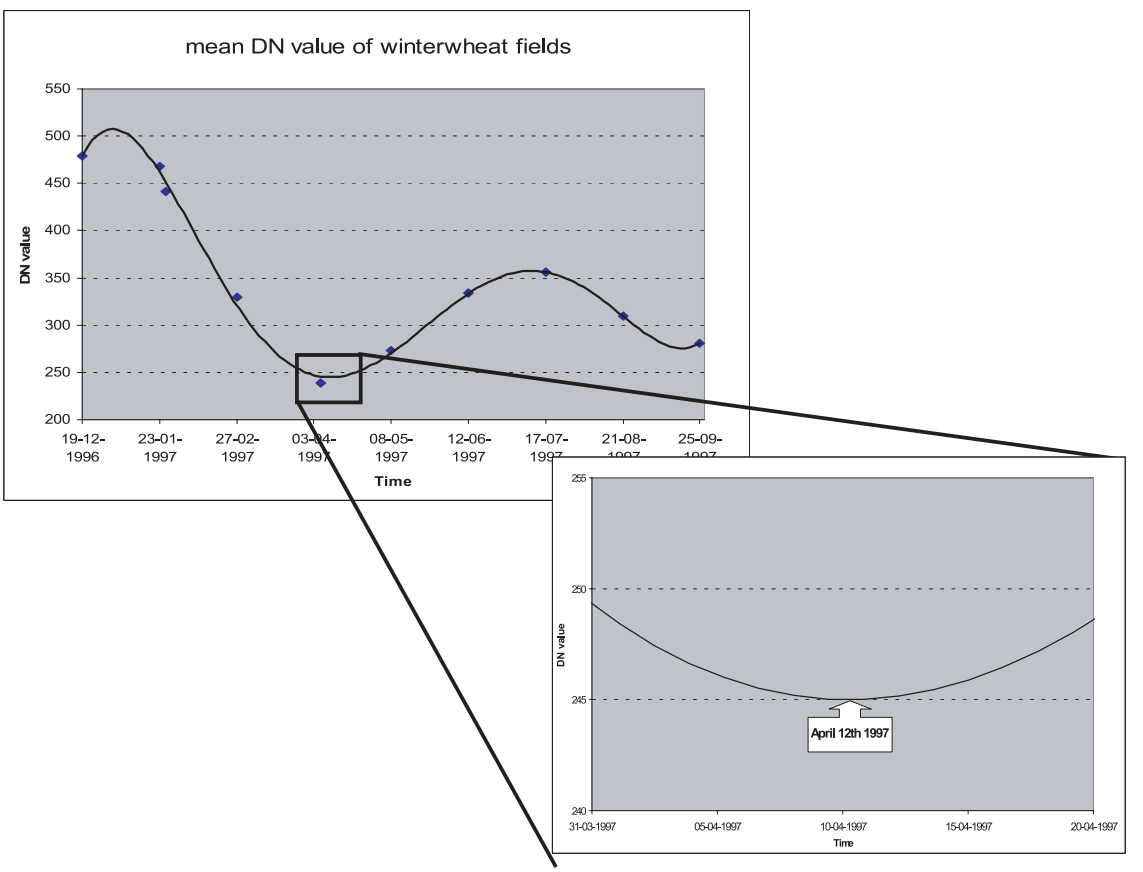

Figure 3. Identification of the date of flowering from the 1996–1997 ERS-SAR time-series.

number of local maximum and minimum values that can be expected for the studied time period. Starting with a local maximum for soil backscattering (only), to a local minimum when the soil backscatter is fully masked at flowering, continuing to a local maximum at maturity with backscatter of the ear layer, towards a local minimum after all the fields have been harvested and a dry soil is exposed at the end of summer. As the harvest starts and progresses in June/July, the curve is increasingly influenced by soil characteristics and less by the crop. Flowering date of the wheat crop was set at the 1st local minimum of

Table V. Calculated regional grain production P (without calibration on observed flowering date in pilot area Alpilles) for the 3 production situations. Values in brackets are standard deviations from the mean.

Scenario	Soil type	Area (ha)	Yield (t ha^{-1})	Production (P) (t)	Regional production (t)
1 Potential	–	3000	11.35 (1.02)	34050	34050
2 Water-limited	1	2700	6.08 (0.51)	16416	
	2	300	5.27 (0.39)	1581	17997
3 Water- and nitrogen-limited	1	2700	4.70 (0.28)	12690	
	2	300	4.19 (0.21)	1257	13947

Table VI. Calculated regional grain production P' (with calibration on remote sensing estimate on regional flowering date) for the 3 production situations. Values in brackets are standard deviations from the mean.

Scenario	Soil type	Area (ha)	Yield (t ha^{-1})	Production (P') (t)	Regional production (t)
1 Potential	–	3000	11.45 (0.19)	34350	34350
2 Water-limited	1	2700	5.84 (0.15)	15768	17274
	2	300	5.02 (0.16)	1506	
3 Water- and nitrogen-limited	1	2700	4.53 (0.08)	12231	13446
	2	300	4.05 (0.08)	1215	

Table VII. Wheat production (1997) in departments 82 and 83, area and average yield (Arvalis, 2003).

Department	Region	Total Production (t)	Area (ha)	Yield (t ha^{-1})
82	Midi-Pyrénées (*MP*)	540600	104400	5.18
83	Provence Alpes-Côte d'Azur (*PAC*)	518500	98100	5.29

the fitted polynomial function, which was closest to April 12th, 1997 or Julian day 101, and in agreement with the calibrated *Rotask* simulation model and field observations (Julian day 105–107).

3.2. Crop growth simulation results

Calibration of *Rotask* resulted in temperature sums between sowing-emergence of 420 °Cd (base temperature of –10 °C), emergence-flowering of 1050 °Cd (base temperature of 0 °C) and flowering-maturity of 850 °Cd (base temperature of 0 °C). On the basis of the flowering date for the region derived from radar remote sensing (April 12th, 1997), the simulated variation in temperature sum between emergence and flowering was 930–1180 °Cd, depending on sowing date in November 1996. This variation was applied to run the model for the 3 production situations.

The simulation results and regional yield estimates (Tabs. V and VI) illustrate the yield-limiting effects of insufficient water and nutrient supply in the absence of irrigation and fertiliser application. Hence, appropriate management (irrigation and fertiliser application) leads to appreciably higher production levels, in the absence of pests and diseases.

From Tables V and VI can be concluded that using field observations or remote sensing estimates of a flowering date give comparable results for yield simulations and that differences can be related to differences in crop management (sowing date and cultivar). This supports the assumption that this method can be used to regionally calibrate the model on phenological characteristics. The decrease in standard deviation for the remote sensing approach (Tab. VI) is caused by the fact that the start of the reproductive (grain filling) phase was fixed at the flowering date estimated from remote sensing (causing a variable temperature sum between emergence and flowering). The use of remote sensing data integrates the effects of varying wheat crop management over the region into one representative value for flowering date. In the original approach (Tab. V), the temperature sum between emergence and flowering was calibrated on field-data in the Alpilles pilot area and then applied with a variable sowing date, which consequently resulted in a variable flowering date.

3.3. Validation

Actual wheat production data of the departments in the *MP* and *PAC* region obtained from Arvalis (Tab. VII; Arvalis, 2003) included total wheat production (t), wheat area (ha) and

average grain yield (t ha^{-1}). The simulated values of 5–6 t ha^{-1} agree well with observed values that are remarkably low (≈50% of their potential). According to Arvalis (op. cit.), average nitrogen application in 1997 was about 100 kg ha^{-1} in the *MP* and *PAC* region, which is about 55% of total crop requirements for realisation of the potential yield of 11.5 t ha^{-1}.

Inadequate water supply may have been limiting yield (if additional irrigation was not applied, especially since 1997 was an extremely dry year), while yield reductions may have resulted from non-controlled pests and diseases. In the simulation model, inadequate water and nitrogen supply was taken into account (production situations 2 and 3), but the regional distribution of crop management practices could not be simulated. Fertiliser application rates of 100 kg N ha^{-1} could be simulated, but information on irrigation rates and dates were not available for the region.

Introducing the effects of local management can be simulated in point-based simulation models, but retrieving the necessary (regional) data is very difficult and requires extensive field work. However, remote sensing data may be used to spatially estimate crop status (e.g. biomass, nitrogen content and moisture status) that may be integrated in the simulation process for run-time calibration (Jongschaap, 2005), but that is beyond the scope of this paper.

4. CONCLUSION

In this paper we present a method to make regional, quantitative production volumes of winter wheat on the basis of spaceborne remote sensing observation in combination with a dynamic crop growth simulation model. The most important conclusions are:

- For purposes of regional winter wheat yield estimations, an approach combining optical and radar remote sensing data with point-based crop growth modelling yields satisfactory results that are in agreement with regional yield statistics. Regional yield production can be estimated at an early stage, even before harvest.
- Flowering dates for wheat crops can be estimated from time-series of C-band radar data, as radar signals are attenuated maximally at the flowering stage. This requires that radar signals from wheat fields can be isolated from those from other fields, which appeared feasible with an accuracy > 80% by combining optical remote sensing data from early winter and late summer.
- Flowering dates for wheat crops that are estimated from time-series of C-band radar data may replace phenological field observations for the use of model calibration and give comparable simulation results. This enables scaling up point models to regional applications without an increase in (phenological) field observations on the ground.
- Use of field-specific flowering dates for simulations within a region would result in more accurate estimates of regional grain production, than the use of one single value for the whole region. This does require however sufficiently large wheat fields. Wheat fields in the *Alpilles* area were medium-sized on average, and therefore it is not certain that an individual field approach would have increased simulation accuracy.
- As the differences between simulated and observed production levels are presumably associated with management practices, such as irrigation and fertiliser application, the use of a remote sensing run-time calibration method for dynamic simulation models (Jongschaap, 2005) may result in increased simulation accuracy.

Acknowledgements: The Alpilles-ReSeDA project was funded by the European Commission (EU-DG XII, contract ENV4-CT96-0326 - PL952071), the French "Program National de Télédétection Spatiale", "Programme de Recherches en Hydrologie" and by the Dutch Ministry of Agriculture, Nature Management and Fisheries through their programmes on precision agriculture. Philippe Desvignes (Arvalis - Institut du Végétal, France) provided the regional wheat data and fertiliser data. We are grateful to Prof. Dr. Steven M. de Jong and Prof. Dr. Herman van Keulen and two anonymous reviewers for useful comments on the manuscript.

REFERENCES

Arvalis (2003) Institut du Végétal, France http://www.arvalisinstitutduvegetal.fr

Attema E.P.W., Ulaby F.T. (1978) Vegetation modelled as a water cloud, Radio Sci. 13, 357–364.

Boegh E., Thorsen M., Butts M.B., Hansen S., Christiansen J.S., Abrahamsen P., Hasager C.B., Jensen N.O., van der Keur P., Refsgaard J.C., Schelde K., Soegaard H., Thomsen A. (2004) Incorporating remote sensing data in physically based distributed agro-hydrological modelling, J. Hydrol. 287, 279–299.

Bouman B.A.M. (1991) Linking X-band radar backscattering and optical reflectance with crop growth models, Ph.D. Thesis, Wageningen Agricultural University, Wageningen, the Netherlands, 167 p.

Bouman B.A.M., Van Kraalingen D.W.G., Stol W., Van Leeuwen H.J.C. (1999) An agroecological modelling approach to explain ERS SAR radar back scatter of agricultural crops, Rem. Sens. Environm. 67, 137–146.

Clevers J.G.P.W., Vonder O.W., Jongschaap R.E.E., Desprats J.F., King C., Prévot L., Brugier N. (2002) Using SPOT data for calibrating a wheat growth model under mediterranean conditions, Agronomie 22, 687–694.

De Wit A.J.W., Clevers J.G.P.W. (2004) Efficiency and accuracy of per-field classification for operational crop mapping, Int. J. Rem. Sens. 25, 4091–4112.

ESA (1998) Vegetation Retrieval by Combining Microwave and Optical Remote Sensing, Final Report ESA/ESTEC, Contract 11154/94/NL/NB(SC), Synoptics, AB-DLO, TNO-FEL and WAU, 113 p.

FAO (1995) Digitized Soil Map of the World and derived Soil Properties (version 3.5), CD-ROM, FAO, Rome.

Guyot G., Baret F., Major D.J. (1988) High spectral resolution: Determination of spectral shifts between the red and the near infrared, Int. Arch. Photogram. Rem. Sens. 11, 750–760.

Hamacher M. (2000) Zustandserfassung von Wintergetreide und Zuckerrüben während des Wachstums mit Hilfe des C-Band Radars der ERS-1 und ERS-2 Satelliten, Ph.D. thesis, Rhine Friedrich Wilhelms University, Bonn, Germany, 114 p.

Hill M.J., Donald G.E., Vickery P.J., Moore A.D., Donnelly J.R. (1999) Combining satellite data with a simulation model to describe spatial variability in pasture growth at a farm scale, Aust. J. Exp. Agr. 39, 285–300.

Jago R.A., Cutler M.E.J., Curran P.J. (1999) Estimating canopy chlorophyll concentration from field and airborne spectra, Remote Sens. Environ. 68, 217–224.

Jones J.W., Keating B.A., Porter C.H. (2001) Approaches to modular model development, Agr. Syst. 70, 421–443.

Jongschaap R.E.E. (1996) *Rotask* 1.0: a simulation model for continuous cropping and tillage systems, Reference manual, Series: Report (70), DLO Research Institute for Agrobiology and Soil Fertility (AB-DLO), Haren, the Netherlands, 41 p. + annexes.

Jongschaap R.E.E. (2000) Calibration and validation of *Rotask v1.5* simulation model on field data of the ReSeDA project in Southern France, with special reference to winter wheat, in: Final report ReSeDA, EU-DG XII, ENV4-CT96-0326 - PL952071, France: BRGM, CESBIO, CETP, INRA (coordinator); Italy: IROE; the Netherlands: WAU, AB-DLO, Synoptics BV; United Kingdom: UC; Spain: UV.

Jongschaap R.E.E. (2005) Run-time calibration of simulation models by integrating remote sensing estimates of leaf area index and canopy nitrogen, Eur. J. Agron. (submitted).

Jongschaap R.E.E., Quiroz R.A. (2000) Integrating remote sensing with process-based simulation models to assess primary production capacity for grazing lands in The Andes, 5th seminar on GIS and developing countries: GISDECO 2000, 2–3 November 2000, Los Baños, Philippines.

Jongschaap R.E.E, Booij R. (2004) Spectral measurements at different spatial scales in potato: relating leaf, plant and canopy nitrogen status, Int. J. Appl. Earth Obs. Geoinform. 5, 205–218.

Lloyd C.D., Berberoglu S., Curran P.J., Atkinson P.M. (2004) A comparison of texture measures for the per-field classification of Mediterranean land cover, Int. J. Rem. Sens. 25, 3943–3965.

Lopez A., Nezry E., Touzi R., Laur H. (1993) Structure detection and statistical adaptive speckle filtering in SAR images, Int. J. Rem. Sens. 14, 1735–1758.

Macelloni G., Paloscia S., Pampaloni P., Ruisia R., Dechambre M., Valentin R., Chanzy A., Prévot L., Bruguier N. (2002) Modelling radar backscatter from crops during the growth cycle, Agronomie 22, 575–579.

Moreau S., Le Toan T. (2003) Biomass quantification of Andean wetland forages using ERS satellite data for optimizing livestock management, Remote Sens. Environ. 84, 477–492.

Prévot L., Baret F., Olioso A., Van Leeuwen H.J.C., Schouten L.S.M., Jongschaap R.E.E. (1998) Assimilation of multi-temporal remote sensing data to monitor vegetation and soil: the Alpilles-ReSeDA project. Proc. IGARSS '98 Symposium, July 1998, Seattle, WA, USA, 3 p.

Prévot L., Chauki H., Troufleau D., Weiss M., Baret F., Brisson N. (2003) Assimilating optical and radar data into the STICS crop model for wheat, Agronomie 23, 297–303.

ReSeDA (2000) Assimilation of multisensor and multitemporal remote sensing data to monitor vegetation and soil functioning, Final report, EU-DG XII, ENV4-CT96-0326 - PL952071; France: BRGM, CESBIO, CETP, INRA (coordinator); Italy: IROE; the Netherlands: WAU, AB-DLO, Synoptics BV; United Kingdom: UC; Spain: UV.

Rouse J.W., Haas R.H., Deering D.W., Schell J.A., Harlan J.C. (1974) Monitoring the vernal advancement and retrogradation (greenwave effect) of natural vegetation. NASA/GSFC Type III Final Report, Greenbelt, MD, USA.

Shupe S.M., Marsh S.E. (2004) Cover- and density-based vegetation classifications of the Sonoran Desert using Landsat TM and ERS-1 SAR imagery, Remote Sens. Environ. 93, 131–149.

Story M., Congalton R.G. (1986) Accuracy assessment: a user's perspective, Photogramm. Eng. Rem. 52, 397–399.

Susan Moran M., Hymer D.C., Qi J., Kerr Y. (2002) Comparison of ERS-2 SAR and Landsat TM imagery for monitoring agricultural crop and soil conditions, Remote Sens. Environ. 79, 243–252.

Synoptics (1996) Integrated Remote Sensing and GIS application, DLO Research Institute for Agrobiology and Soil Fertility (AB-DLO), TNO Physics and Electronics laboratory and Wageningen Agricultural University, the Netherlands, Vegetation retrieval by combining microwave and optical remote sensing, ESTEC Contract 11154/94/NL/NB(SC).

Thenkabail P.S., Smith R.B., De Pauw E. (2000) Hyperspectral vegetation indices and their relationship with agricultural crop characteristics, Remote Sens. Environ. 71, 158–182.

Van Ittersum M.K., Rabbinge R. (1997) Concepts in production ecology for analysis and quantification of agricultural input-output combinations, Field Crops Res. 52, 197–208.

Van Leeuwen H.J.C. (1996) Methodology for combining optical and microwave remote sensing in agricultural crop monitoring: The sugar beet as special case, Ph.D. thesis, Wageningen Agricultural University, The Netherlands, 248 p.

Vermote E.F., Tanré D., Deuzé J.L., Herman M., Morcrette J.J. (1997) Second simulation of the satellite signal in the solar spectrum, 6S: An overview, IEEE T. Geosci. Remote 35, 675–686.